Journal of the Iranian Chemical Society (2023) 20:2257–2268
https://doi.org/10.1007/s13738-023-02831-9

ORIGINAL PAPER

Folic acid and carbon dots-capped mesoporous silica for pH-responsive targeted drug delivery and bioimaging

Marziyeh Poshteh Shirani[1] · Ali A. Ensafi[1] · Behzad Rezaei[1] · Zahra Amirghofran[2]

Received: 13 October 2022 / Accepted: 19 May 2023 / Published online: 8 June 2023

Abstract

Multifunctional nanocarriers are presently used to solve crucial unmet challenges in cancer treatment. In this project, we reported an intelligent amine mesoporous silica (MSN-NH_2)-based nanocarrier with a potent fluorescence emission and imaging capacity for the delivery of the payload to the tumor cells. Gemcitabine (GEM)-loaded MSN-NH_2 has been used as a drug model. Hydroxyl and carboxylic acid carbon dots (CDs) were used to electrostatically coat the surface of MSN-NH_2@GEM to yield biocompatible CDs-capped MSN-NH_2 (CDs/MSN-NH_2@GEM). Folic acid (FA) was covalently grafted onto the carboxyl groups of CDs/MSN-NH_2@GEM to form (FA/CDs/MSN-NH_2@GEM) to deliver the nanocarrier to the site of action. GEM release from the formulation is sustained and dependent on pH (pH 5.4 > pH 7.4), according to the in vitro release assessment at different pH values. FA-targeted CDs/MSN-NH_2@GEM developed had higher cytotoxicity compared with the non-targeted NPs in HeLa and K562 (human cervical carcinoma and chronic myeloid leukemia cell lines, respectively), as shown by the MTT assay. Fluorescence microscopic images and flow cytometry assay were used to comprehend anticancer activity and express targeting ability and cellular uptake FA/CDs/MSN-NH_2@GEM toward the HeLa cancer cells. Moreover, molecular docking was used to evaluate the interactions of GEM molecule with the human deoxycytidine kinase (dCK). The present study may present a new understanding of the development of targeted, intelligent CDs-capped MSN-NH_2-based hybrid materials in cancer therapy.

✉ Ali A. Ensafi
ensafi@iut.ac.ir; aensafi@uark.edu; aaensafi@gmail.com

[1] Department of Chemistry, Isfahan University of Technology, Isfahan 84156-83111, Iran

[2] Autoimmune Disease Research Center, Department of Immunology, School of Medicine, Shiraz University of Medical Sciences, Shiraz, Iran

Graphical abstract

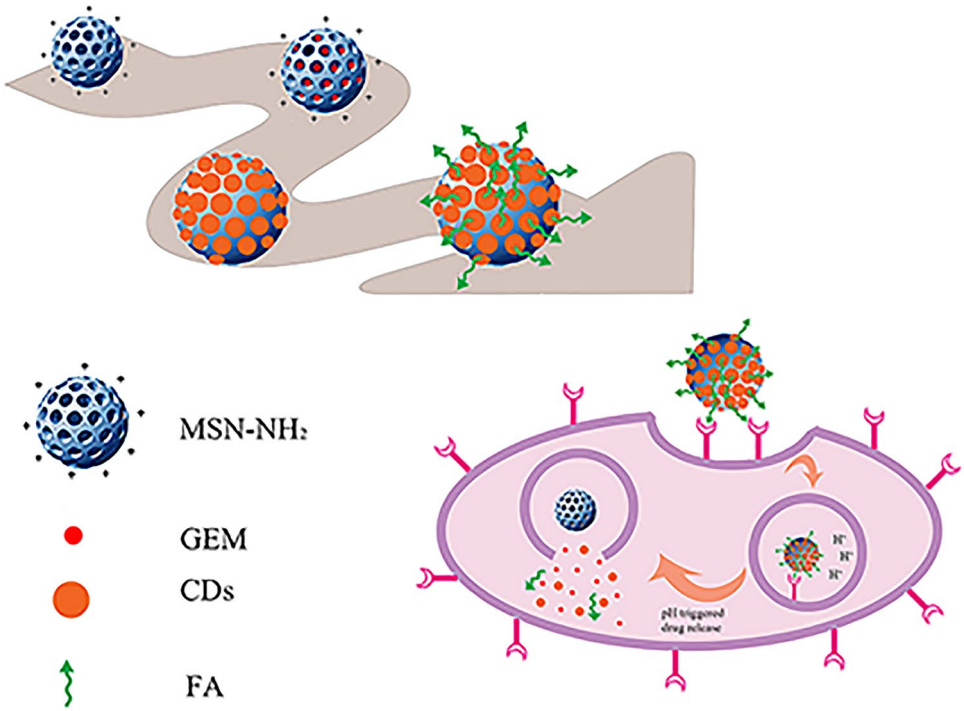

Keywords Mesoporous silica · Gemcitabine · Carbon dot · Bioimaging · Molecular docking

Introduction

Cancer is still one of the fatal diseases in the universe despite the extraordinary growths in the knowledge of the disease. Chemotherapy is the conventional treatment method for cancer. Some of the drawbacks of tumor chemotherapy include poor targeting and terrible side effects on normal tissues [1–4]. Therefore, it is crucial to design an effective drug delivery system to deliver the desired drug with no loss or leakage before reaching the corresponding cells or tissues. The delivery system must be capable of leading the drug molecules into tumor cells with no premature drug leakage for this purpose [5]. Silica nanoparticles have been particularly attractive among different nanocarriers for drug delivery. In addition, these nanoparticles have received FDA approval for human use in clinical tests [6]. Mesoporous silica nanoparticles (MSNs), which are applied as drug delivery systems, have different considerable properties such as ordered arrays of two-dimensional hexagonal mesoporous structures, highly ordered channels, uniform particle sizes, extensive surface areas, high pore volumes, adjustable pore diameters, and facile surface functionalization [7–9]. More significantly, MSNs can also function as supports for incorporation with fluorescent and magnetic compounds for diagnostic applications. Various MSN-based drug delivery systems have been developed using nanoparticles, linear molecules, multilayers, and macrocyclic compounds as "gatekeepers" over the MSN pore entrance, which can be stimulated by redox potentials, temperature or pH variations, or photoirradiation to release drugs as needed [10–13]. Such different molecules as synthetic polymers [14], amino acids [15], peptides, nucleic acids, quantum dots (QDs) [16], inorganic NPs [9], natural polymers, or their derivatives [17], have reportedly been used as gatekeepers to provide intelligent control for the escape of the encapsulated molecules from the silica channels.

Carbon dots (CDs), a new group of luminescent carbon-based compounds, with diameters of up to 10 nm have newly been of great interest in the areas of clinical diagnosis, bioimaging, and catalysis [18–20]. CDs with graphitic structures have physicochemical characteristics similar to semiconducting quantum dots. Given their superior properties such as non-toxicity, good solubility in water, exceptional photostability, adjustable surface functional groups, great cell membrane permeability, and high biocompatibility in comparison with the traditional QDs and organic dyes based on heavy metals, CDs are considered superior candidates for fluorescence bioimaging [21–23]. CDs have previously been used as bioimaging agents rather than drug delivery controls. Due to their 2–10 nm range diameter, CDs can be

employed as gatekeepers to cap the MSN pores to control the on-demand drug release.

The main disadvantages of cancer chemotherapy are the incapability to differentiate between the cancerous and normal cells and low accumulation of the drug inside tumor tissue, which gives rise to adverse side effects and high dosage injections [24, 25]. Successful treatment can be achieved by special drug targeting delivery, which can decrease the undesirable side effects of drugs and improve the efficiency of the therapy [26]. Some of the compounds previously used as targeting agents include different ligands such as small chemical molecules, peptides, aptamers, and monoclonal antibodies [27–29].

Folic acid (FA) is a small molecule, which is stable over a broad range of temperatures and pH values, cheap and non-immunogenic. Furthermore, folic acid is capable of binding to the folate receptor (FR) following connection to the drugs or diagnostic markers [30]. FR is overexpressed on the outside surface of some cancer cells, as biological studies show. The facilitation of the cellular uptake of the FA modified nanosystems and following cell apoptosis by a receptor-mediated via the attachment of FA with FR positive cancer cells have been previously reported [31, 32].

Gemcitabine (GEM) is a water-soluble pyrimidine antimetabolite as a chemotherapeutic agent to treat solid pancreas, neck, head, breast, bladder, colon, and ovary cancers and other solid tumors [33–36]. However, a short half-life of 8–17 min. in human plasma is caused by the fast deamination of gemcitabine. Thus, to maintain the therapeutic level of gemcitabine, it must be administered in high dosages. Gemcitabine is presently administered at a high dosage of 1000 mg/m^2 for 30 min by intravenous (i.v.) injection, which leads to hematotoxicity and other side effects, to reach a therapeutic level [37]. Consequently, it is highly necessary to prepare gemcitabine with good plasma stability. Different drug delivery approaches, including the application of micelles, liposomes, and silica nanoparticles, have been reportedly used to overcome the obstacles pointed out [38–40].

The design of a multi-functional drug delivery system, which involves the introduction of a pH-sensitive drug carrier of nano-size with bioimaging capability, is reported in this work. Gemcitabine was loaded into amine-functionalized mesoporous silica (MSN-NH_2@GEM), followed by coating with CDs (CDs/MSN-NH_2@GEM). Afterward, folic acid (FA) was grafted to the surface of nanoparticles in order to specifically target folate receptor overexpressing cancer cells (FA/CDs/MSN-NH_2@GEM). The photoluminescence characteristics, morphology, zeta potential, size distribution, drug encapsulation efficiency, and in vitro release profile were also investigated. In addition, the in vitro cytotoxic activity of the formulation prepared was assessed on HeLa and K562 cells. Ultimately, the nanoformulation was shown to provide excellent potential for real-time imaging for monitoring cellular tracking during tumor treatment. Also, the interaction of the GEM and human deoxycytidine kinase (dCK) was investigated by molecular docking.

Materials and methods

Materials

Tetraethyl orthosilicate (TEOS), *N*-cetyltrimethylammonium bromide (CTAB), folic acid (≥ 97%), N-hydroxysuccinimide (NHS), and 3-[4,5-dimethyl-thiazol-2-yl]-2,5-diphenyltetrazolium bromide (MTT) were provided by Sigma-Aldrich Chemical Co. Gemcitabine (GEM) was purchased from Sobhan Oncology Co., Ltd. (Gilan, Iran). N-(3-dimethylaminopropyl)-N-ethyl carbodiimide hydrochloride (EDC) and 3-aminopropyltriethoxysilane (APTES) were supplied by Merck Chemical Co. Trypsin, Roswell Park Memorial Institute (RPMI) 1640 medium, penicillin/streptomycin, and fetal bovine serum (FBS) were purchased from Gibco (Germany). Other material and solvents were of analytical grade and applied as received.

K562 and HeLa cell lines were obtained from the National Cell Bank of Iran, Pasteur Institute of Iran. The cells were cultured in RPMI 1640 medium containing 10% FBS, 1% (v/v) penicillin and 1% (v/v) streptomycin at 37 °C in a humidified atmosphere containing 5% CO_2.

Characterization

Jasco FP-750, V–570 and 680-plus (Japan) instruments were used to record the fluorescence; UV–Vis, and Fourier transform infrared (FT-IR) spectra, respectively. An Asenware AW-XDM300 (Chain) diffractometer was employed to record XRD patterns using Ni-filtered CuKα radiation. Field emission scanning electron microscopy (FE-SEM) was used to study the appearance of nanoparticles using a QUANTA FEG 450 instrument (USA) at an accelerating voltage of 20 kV. A Philips CM30 300 kV instrument (Netherlands) was used to record transmission electron microscopy (TEM) images. Dynamic light scattering (DLS) measurements and zeta (ζ)-potential were applied to determine the hydrodynamic diameter of the nanoparticles and evolution of the surface charge, respectively, using HORIBA SZ-100 instruments (Japan). A BELSORP-II system (Japan) was employed to monitor the nitrogen adsorption–desorption isotherms at – 196 °C. Raman spectra were recorded using a Tanso Raman spectrophotometer (Iran).

Synthesis of NH_2-modified MSN

A modified literature method was used to synthesize the amino-functionalized MSN (MSN-NH_2) nanoparticles [40]. In short, 0.10 g of CTAB was dissolved in 48 mL of deionized water, followed by the addition of 0.030 g of NaOH and adjusting the solution temperature at 70 °C. TEOS (400 µL) and ethyl acetate (1 mL) were then injected dropwise to the solution. Afterward, the amine was introduced to MSN by adding 80 µL of APTES to the above solution. The reaction was continued for 3 h at 70 °C. The solid product was collected by centrifugation and purified by rinsing with ethanol. For template extraction, the product was dispersed in a MeOH/HCl mixture (16 mL/1 mL) and refluxed at 60 °C for 24 h to remove the surfactant template (CTAB). Eventually, the MSN-NH_2 was collected by centrifugation, rinsed several times with ethanol, and dried *in vacuo* at 60 °C overnight.

Loading of GEM into the NH_2-modified MSN

5.0 mg of MSN-NH_2 was suspended with 2 mL of a 5 mg/mL solution of GEM, and the suspension thus obtained was stirred at ambient temperature for 24 h. The GEM encapsulated MSN-NH_2 was then centrifuged at 12,000 rpm for 10 min. The supernatant was collected to assess the loading capacity (DL) and encapsulation efficiency (EE) of the drug, and the quantity of free GEM was spectrophotometrically determined at 270 nm utilizing a standard GEM solution calibration curve. The DL and EE of GEM loaded onto MSN-NH_2 were founds as follows:

$$\mathrm{DL}(\%) = \frac{\text{Total weight of GEM} - \text{Free GEM weight in supernatant}}{\text{Mass of final formulation}} \times 100$$

$$\mathrm{EE}(\%) = \frac{\text{Total weight of GEM} - \text{Free GEM weight in supernatant}}{\text{Total weight of GEM}} \times 100.$$

Synthesis of CDs and CDs@MSN-NH_2

Carbon dots were obtained from Laurus nobilis using one-step hydrothermal method. The Laurus nobilis collected was first rinsed with water to remove the impurities, followed by drying at ambient temperature. Afterward, the leaves were powdered, and 0.50 g of the resulting powder was mixed with 40 mL of distilled water. Having been stirred for 20 min., the mixture was transferred into a Teflon-lined stainless steel autoclave and heated at a fixed temperature of 180 °C for 12 h. The autoclave was then cooled to ambient temperature. The product was centrifuged at 12,000 rpm for 5 min. To remove the unreacted compounds from the CDs solution, it was transferred into a dark container and stored at 4 °C. 1.0 mL of a 5 mg/mL suspension of GEM-loaded MSN-NH_2 was added to 1.0 mL of CDs, and the resulting mixture was stirred at ambient temperature for 24 h. CDs/MSN-NH_2 hybrid preparation and capping of MSN-NH_2 pores with CDs result from the electrostatic interactions between the amine groups on the silica surface and the hydroxyl and carboxylic groups on the CDs.

Preparation of aminated-FA and FA/CDs/MSN-NH_2

1.0 mmol of a solution of FA in 10 mL of DMSO was incubated with 1.0 mmol of EDC and 2.0 mmol of NHS at ambient temperature for 20 h. 200 µL of pyridine and 200 µL of ethylenediamine were then added to the above mixture, and the reaction was continued at ambient temperature overnight. The aminated FA was precipitated using excess acetonitrile and rinsed with acetonitrile to eliminate the residue. The precipitate formed was freeze-dried for 24 h and kept at − 20 °C [41].

5.0 mg of CDs/MSN-NH_2 were suspended in 10 mL of phosphate buffered saline (PBS) at pH 7.4 to attach CDs/MSN-NH_2 to FA. Afterward, 15.0 mg of EDC and 5.0 mg of NHS were added under constant stirring over a period of 1 h. Aminated FA was then added, and the mixture obtained was stirred overnight. FA/CDs/MSN-NH_2 was collected by centrifugation at 12,000 rpm for 10 min, washed three times with DI water, and dried *in vacuo* overnight.

2.7, In vitro drug release.

GEM-loaded MSN-NH_2 and 1.0 mL of GEM-loaded CDs/MSN-NH_2 were placed into a sealed dialysis membrane (cutoff = 3500 Da), which was then soaked in citrate buffer (pH = 5.4) and PBS (pH = 7.4) on a shaker incubator set at 60 rpm at 37 °C. 1.0 mL aliquots were then taken at specific time points and replaced with an equal quantity of the released buffers. Ultimately, UV–Vis spectroscopy was applied to analyze the GEM concentration in the samples at 269 nm. All the experiments were carried out in triplicate.

In vitro cytotoxicity assay

MTT assay was employed to investigate the cytotoxicity of the free GEM, CDs, free FA/CDs/MSN-NH_2, and GEM-loaded CDs/MSN-NH_2 in the absence or presence of FA

against HeLa and K562 cells. The cells were seeded in 96-well plates at 7000 cells per well and maintained in a humidified 5% CO_2 incubator at 37 °C for 24 h. The control samples included the untreated cells. The next day, the cells were exposed to free GEM, targeted and non-targeted GEM-loaded CDs/MSN-NH_2. Following incubation for 24 h, the cells were exposed to 20 µL of 5.0 mg/mL MTT in PBS and maintained at 37 °C for 3 h. The medium was then discarded, and 100 µL of DMSO was added to each well to dissolve the formazan crystals. The plate was shaken for 10 min at 600 rpm, and then, the absorbance was measured at 570 nm with a reference wavelength at 630 nm using a microplate reader The percentage of cell viability was determined using the following equation.

$$\text{Cell Viability (\%)} = \frac{(A_{570} - A_{630})\text{treated cells}}{(A_{570} - A_{630})\text{control cells}} \times 100.$$

Apoptosis analysis by flow cytometry

Flow cytometry was used to assess the apoptotsis induction using annexin V and propidium iodide (PI) staining. In short, HeLa cells were seeded in 6-well plate (1×10^5 cells per well) and maintained in a humidified 5% CO_2 incubator at 37 °C overnight. The cells were then treated with GEM-loaded CDs/MSN-NH_2 and FA/CDs/MSN-NH_2 for 24 h at 37 °C. Afterward, the cells were rinsed with cold PBS, trypsinized, centrifuged, and then suspended in Annexin V buffer. Next, the cells were stained with 50 µg/ml PI solution and incubated for 20 min in the dark. A flow cytometer (Becton Dickinson, USA) was eventually used to analyze the treated cells. The cells at the upper and lower right quadrants were considered as apoptotic cells while those at the upper left were necrotic.

Cellular uptake analysis by fluorescent microscopy

Cellular uptake was qualitatively evaluated using fluorescence microscopy. HeLa cells (5×10^4 cells per well) were seeded in 12-well plates and maintained overnight at 37 °C under 5% CO_2 atmosphere. The cells were then treated with GEM-loaded CDs/MSN-NH_2 and FA/CDs/MSN-NH_2 for 4 h at 37 °C. The culture medium was finally discarded, and the cells were rinsed three times with PBS and visualized using a Micros fluorescence microscope (Austria).

Molecular docking

The chemical structure of GEM was optimized using Gaussian 09 at the level of B3LYP/6-311G++. The crystal structure of the dCK (PDB ID: 2NO0) was taken from the protein databank (http://www.rcsb.org/pdb). Molecular docking studies were performed using the Autodock Vina [42] using the Lamarckian genetic algorithm [43]. The structure of GEM molecules, water molecules, the heteroatoms, and chain B dCK were removed from the PDB files. Standard values were used for all the docking parameters. LIGPLOT + [44], which is a program for automatically plotting protein–ligand interactions, was used in the analysis of the interactions between dCK with the GEM molecule. The UCSF Chimera [45] packages were used to produce the molecular image.

Results and discussion

Synthesis and characteristics of CDs and Silica NPs

Figure 1 shows the preparation method for FA/CDs/MSN-NH_2 smart nanocarrier. MSN-NH_2 was prepared in an aqueous system containing TEOS and CTAB as the Si precursor and surfactant, respectively. Having been vigorously stirred at 70 °C for 30 min., APTES was injected to the reaction mixture, which was then stirred for 3 h at 70 °C to yield amine-functionalized MSNs. The hydrothermal route was used to prepare the CDs. MSN-NH_2 was then modified with CDs as the gatekeeper groups by electrostatic adsorption. The aminated FA was eventually attached to CDs/MNS-NH_2 by amide bond formation.

In the UV–Vis spectra of CDs (Fig. S1), the absorption band at 280 nm is related to the π-π* transitions of –C=C– bonds and–C=O. As Fig. S2 shows, the emission peaks shift to longer wavelengths in the emission spectra of CDs as the excitation wavelengths increases. The CDs are spherical and well dispersed, based on the TEM image (Fig. S3). As observed in Fig. S3, the average diameter of CDs was estimated at 3 nm. In addition, the DLS test was used to estimate the hydrodynamic size as 3.1 ± 0.5 nm (Fig. S4). Furthermore, the zeta potential of CDs was calculated as − 26.8 ± 1.2 mV. Two diffraction peaks are observed at about 22 and 42° in the XRD pattern of the CDs, which are due to the graphite lattice spacings of (002) and (100), respectively (Fig. S5), verifying the crystalline graphite-like structure of the synthetic CDs [31]. The vibrational peaks at about 1395, 1590, and 3360 cm^{-1} are ascribed to the corresponding aromatic skeletal of C=C, aromatic amine, and hydroxyl and carboxyl groups, respectively, as observed in Fig. S6. Two bands are observed in the Raman spectra of CDs (Fig. S7) at about 1390 and 1600 cm^{-1}, which are due to the D and G bands, respectively [46].

FT-IR confirmed the successful synthesis of MSN-NH_2 and FA/CDs/MSN-NH_2. Figure 2 shows the FT-IR spectra of MSN-NH_2 and FA-CDs-MNS-NH_2. The peak observed at 950 cm^{-1} in the FT-IR spectrum of MSN-NH_2 corresponds to Si–O bond vibration. In addition, the bands around 790

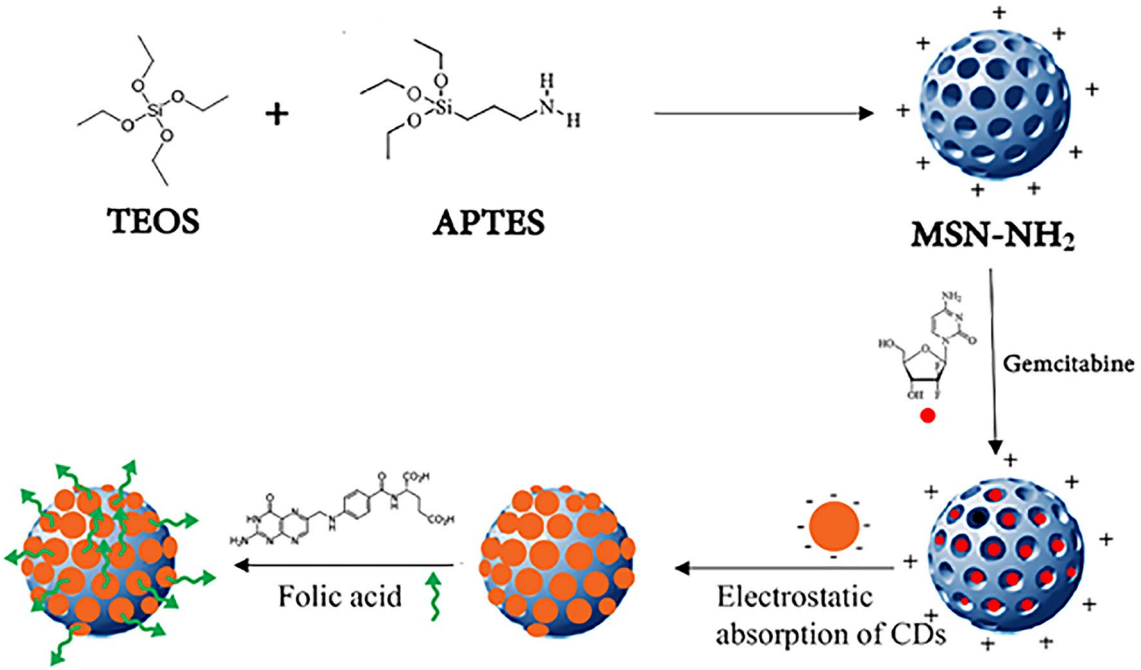

Fig. 1 Schematic representation of the preparation of the pH-responsive FA/CDs/MSN-NH_2 nanocarrier

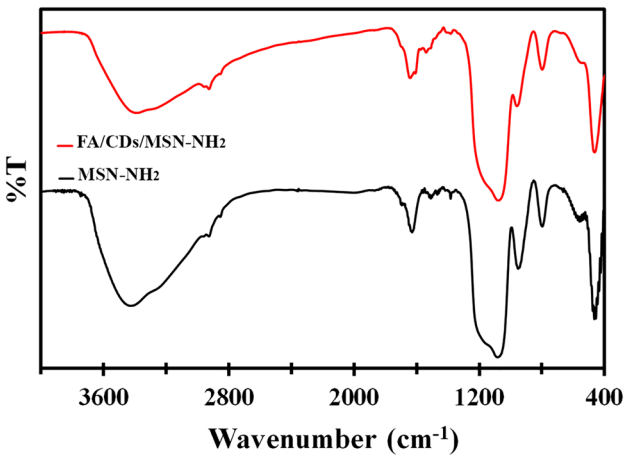

Fig. 2 FT-IR spectra of MSN-NH_2, and FA/CDs/MSN-NH_2 (range of 400–4000 cm^{-1})

and 1070 cm^{-1} are related to the symmetric and asymmetric stretching vibrations of the Si–O–Si bond, respectively. The peak at approximately 1380 cm^{-1} is associated with the stretching vibration of the C–N bond. The absorption bond around 2920 cm^{-1} is due to the CH in CH–NH. The characteristic bands at 3300 and 1510 cm^{-1} are ascribed to the stretching vibration of N−H [40]. The characteristic bands of FA/CDs/MSN-NH_2 conjugates observed at 1650 and 1530 cm^{-1} correspond to the amide bond formed between amine-FA molecules and CDs/MSN-NH_2. The UV–Vis spectra of GEM, CDs/MSN-NH_2, and GEM-loaded CDs/

Table 1 The zeta potential and DLS of the nanoparticles in water

Sample	Zeta	Polydispersity index	Size in water (nm)
MSN-NH_2	+35.5	0.04	170.3
CDs/MSN-NH_2	−1.5	0.13	179.1
FA/CDs/MSN-NH_2	−16.2	0.63	187.5

MSN-NH_2 are shown in Fig. S8. It can be observed that the GEM-loaded CDs/MSN-NH_2 has a characteristic peak at λ = 270 nm. The fluorescence emission spectra of CDs and CDs/MSN-NH_2 are shown in Fig. S9. The fluorescence emission spectra were recorded in the range of 430–700 nm by choosing an excitation wavelength of 420 nm. The CDs had a sharp emission peak at ~ 503 nm. After interaction with MSN-NH_2, there was a slight redshift (~ 4 nm) and enhanced intensity in emission, which demonstrated the successful interaction of CDs with MSN-NH_2. While the emission peak was slightly shifted, it also improved and became sharp and strong in intensity. Furthermore, the size distribution of MSN-NH_2, CD/MSN-NH_2, and FA/CDs/MSN-NH_2 determined by DLS (Table 1) indicates an increase in the size of MSN-NH_2's upon modification.

Figure 3A shows the FE-SEM image of MSN-NH_2 nanoparticles. The nanoparticles appear to have uniformly spherical shapes with an average size of 56 nm. Uniformly spherical shapes and proper size distribution with an average size

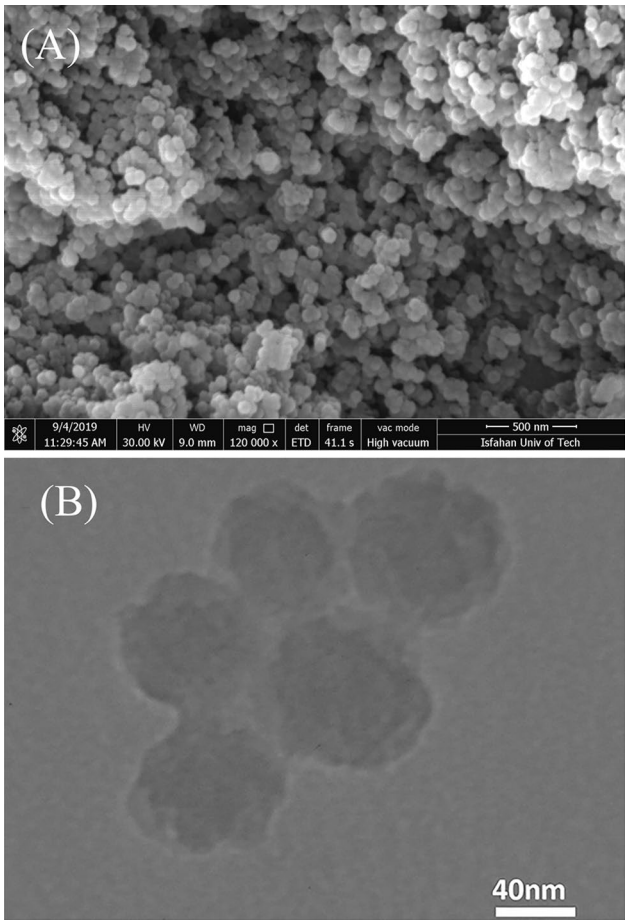

Fig. 3 **A** FE-SEM image of MSN-NH_2 and **B** TEM image of FA/CDs/MSN-NH_2

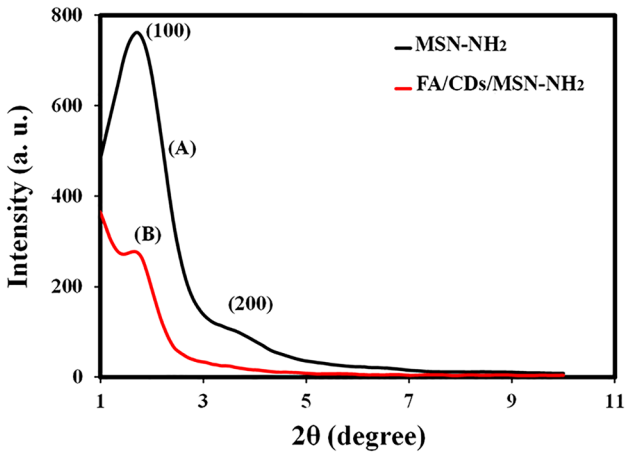

Fig. 4 Low-angle powder XRD of **A** MSN-NH_2 and **B** FA/CDs/MSN-NH_2

of 70 nm are observed in the TEM image of FA/CDs/MSN-NH_2 (Fig. 3B). In addition, the difference between the hydrodynamic diameters of the FA/CDs/MSN-NH_2 dissolved in water, and their actual size is responsible for the different results acquired from DLS and TEM characterizations.

The two major peaks observed at $2\theta = 1.5°–6°$ in the low-angle XRD diffractogram of the MSN-NH_2 correspond to the (100) and (200) crystal planes, respectively (Fig. 4), confirming the hexagonal structure of MSN-NH_2 [40]. The considerable reduction in the diffraction peak intensities of the low-angle XRD pattern of FA/CDs/MSN-NH_2 (Fig. 4) indicates the efficient coverage of the pore openings of MSN-NH_2 by the CDs.

BET analysis was carried out to study the porous nature of MSN-NH_2 and CDs/MSN-NH_2 synthesized. Characteristic type IV isotherms are shown by amine-functionalized MSN (Fig. 5), by the nitrogen adsorption–desorption experiments indicate, which is an indication of the presence of mesoporous structures. Table 2 summarizes the surface areas and pore sizes of the MSN-NH_2 and CDs/MSN-NH_2. The capping of mesoporous silica pores by CDs is verified by the considerable reduction in the surface area of CDs/MSN-NH_2 and disappearance of the maximum peak in the BJH pore size distribution plot compared with plain amine-functionalized MSN.

Drug loading and release study

Following the synthesis of amine-functionalized MSN; gemcitabine was loaded into MSN-NH_2 channels (Fig. 1). MSN-NH_2 channels were coated and capped by negatively charged CDs via electrostatic interaction with the amine groups to entrap and control the release of GEM from nanoparticles. The electrostatic interaction between the carboxylic acid and hydroxyl groups of CDs and amine groups on silica surface presumably controls the drug release in response to exterior pH stimulant. The loading and release profiles are monitored by UV–Vis analysis by comparison with the standard GEM curve. The encapsulation efficiency and loading capacity of the nanoformulations were determined to be $72.0\% \pm 2.68$ and $1.49\% \pm 0.08$, respectively. In vitro drug release survey was performed at pH values of 7.4 and 5.4, applying phosphate and citrate buffers, respectively. The initial burst release within the first 6 h in both buffers (PBS, pH 7.4, and citrate, pH 5.4) is mostly similar in CDs/MSN-NH_2@GEM formulation (Fig. 6).

Nevertheless, a considerable increase in the GEM release rate in citrate buffer and further acceleration in 168 h (31% of the total load *vs*. 18% in PBS; Fig. 6) are shown after 24 h. Moreover, the release pattern of GEM from MSN-NH_2@GEM was evaluated at pH values of 7.4 and 5.4. No similar drug release patterns of GEM form MSN-NH_2@GEM *vs*. CDs/MSN-NH_2@GEM are observed. During 168 h, only 31% and 18% of GEM are released from the CDs/MSN-NH_2@GEM in values of pH 5.4 and 7.4 PBS, respectively, as previously pointed out. This is due to the

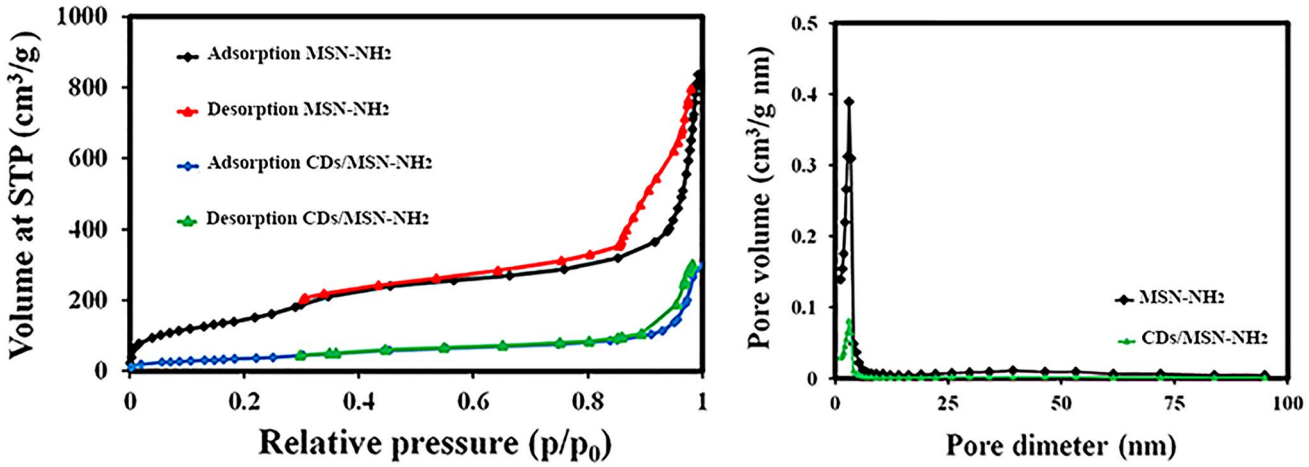

Fig. 5 **A** N_2 adsorption/desorption isotherms and **B** pore size distribution curves of MSN-NH_2, and FA/CDs/MSN-NH_2

Table 2 Structural parameters of MSN-NH_2, and FA/CDs/MSN-NH_2

Sample	BET surface area (m^2/g)	BET pore volume (cm^3/g)	BJH pore diameter (nm)
MSN-NH_2	514.26 ± 5.8 m^2/g	1.26 cm^3/g	3.1 nm
CDs/MSN-NH_2	237.28 ± 3.6 m^2/g	0.50 cm^3/g	–

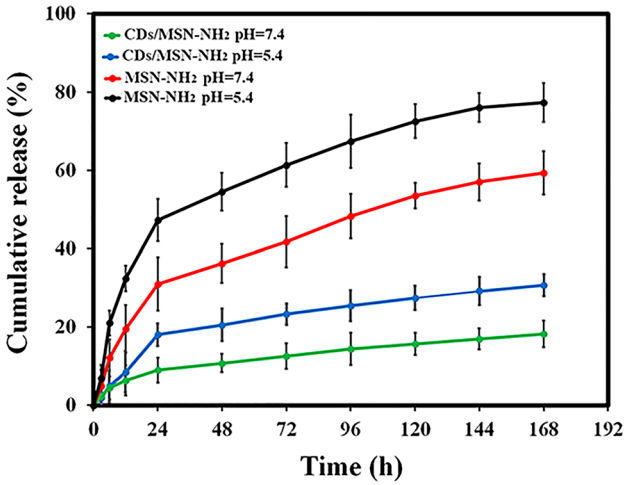

Fig. 6 Gemcitabine (GEM) release profile of MSN-NH_2, CDs/MSN-NH_2 in PBS (pH 7.4), and citrate buffer (pH 5.4)

GEM encapsulation inside the MSN-NH_2 pores and efficient capping of silica channels with CDs. However, 59 and 77% of GEM are released in PBS and citrate buffer, respectively, by MSN-NH_2@GEM without CDs gatekeeper during 168 h. MSN-NH_2@GEM releases GEM remarkably faster at pH 5.4 compared with CDs/MSN-NH_2@GEM. The silica channels are presumably covered and capped by CDs under physiological conditions (pH 7.4). However, positively charged hydrogen ions, which are abundant in citrate buffer (pH 5.4), interact with carboxylate and hydroxyl group of CDs and are protonated. Therefore, the electrostatic interaction between the surface amine groups and carboxylate and hydroxyl groups of CDs could be disturbed through competitive the binding with H^+, leading to GEM release as a result. In addition, the repulsive interaction between the protonated amine on the surface of silica and its analog in gemcitabine molecule complicates the release of entrapped GEM molecules in the MSN-NH_2 pores. Consequently, this type of the delivery system, which applies pH as a trigger for drug release, guarantees that the gatekeeper delays the drug release via the circulation of coated drug carriers in the bloodstream. However, loaded cargos are released from nanoparticles in the tumor proximity and cytosol under acidic conditions immediately after the arrival of the nanoparticle at the tumor microenvironment through the EPR effect and their entrance into the desirable target cell via endocytosis. Given the abundance of hydrogen ions in the endosome, the pH interior of this cellular organ is evaluated as 5.0, which is lower than that of the cytosolic ambiance in a cell. Therefore, the intracellular performance of delivery systems can be figured out by studying their in vitro release behavior [47, 48].

Cytotoxicity assay

MTT assay was used to estimate the in vitro cytotoxicity of CDs and plain FA/CDs/MSN-NH_2 in HeLa and K526 cell lines firstly since the carrier backbone should have low biological toxicity. As observed in Fig. 7A, B, following treatment with CDs and FA/CDs/MSN-NH_2 for 24 h at high concentrations such as 200 μg mL^{-1}, the cell viability is maintained above 86%. The results obtained show the low

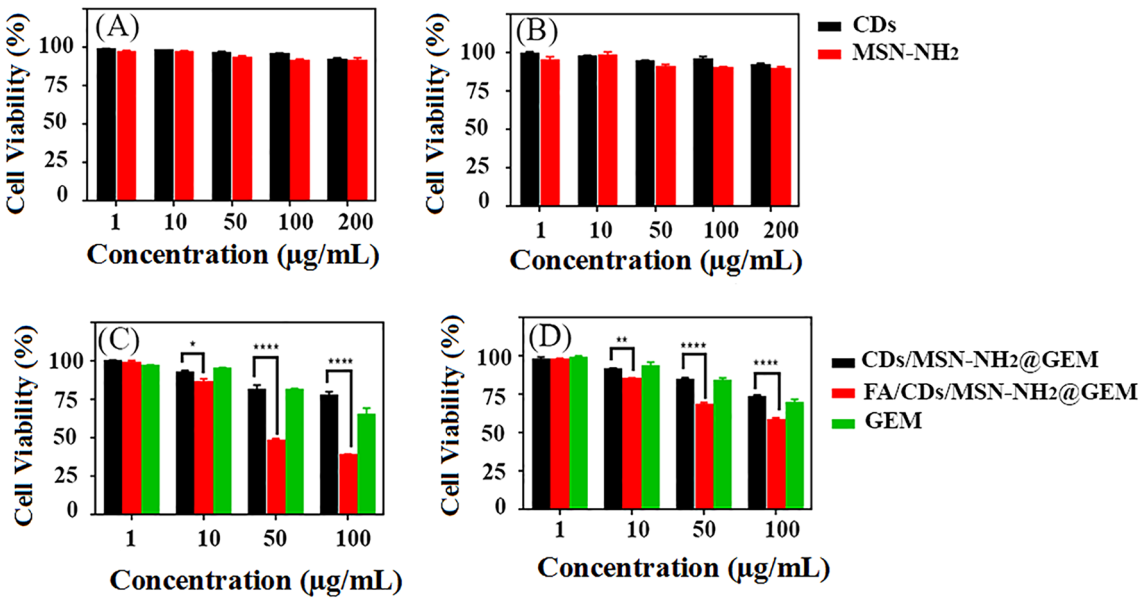

Fig. 7 In vitro cytotoxicity assessment of CDs and MSN-NH_2 after 24 h incubation in **A** HeLa cells and **B** K562 cells, and cytotoxicity assessment GEM, CDs/MSN-NH_2@GEM and FA/CDs/MSN-NH_2@GEM after 24 h incubation in **C** HeLa cells and **D** K562 cells

cytotoxicity of CDs and FA/CDs/MSN-NH_2 and verify their suitability for biomedical applications. Furthermore, the cytotoxic activities of the free GEM, GEM-loaded CDs/MSN-NH_2, and GEM-loaded FA/CDs/MSN-NH_2 on the HeLa and K562 cell lines were investigated. The cytotoxicities of FA-targeted and non-targeted GEM-loaded nanocarriers in HeLa and K562 cell lines are significantly different, as observed in Fig. 7C, D. Based on the MTT results, high cellular uptake of FA/CDs/MSN-NH_2@ GEM and significant cell apoptosis are shown by HeLa cells in comparison with K562 cells. Thus, HeLa cells express higher folate receptors and more susceptibility to FA/CDs/MSN-NH_2@ GEM compared with K562 cells. In brief, FA improves the drug delivery and encapsulation to tumor cells that have high expression of folate receptors. More FRs are expressed in HeLa cells in comparison with low expression of FR at the surface of K562 cells, leading to the more uptake of FA/CDs/MSN-NH_2 via acting endocytosis mediated by FA–FR interaction [49, 50]. Thus, stronger cell inhibition activity is shown by FA/CDs/MSN-NH_2@ GEM on HeLa cells compared with K562 cells.

Apoptosis analysis by flow cytometry

The cells were double stained with Annexin V and PI and analyzed by flow cytometry to assess the apoptosis/necrosis inducing effect of FA/CDs/MSN-NH_2@ GEM and CDs/MSN-NH_2@GEM on HeLa cells. As the results of the studies indicate, the main mechanism of cell death induced by chemotherapeutic drugs is through the apoptosis pathway [51–53]. As shown in Fig. 8, CDs/MSN-NH_2@GEM nanoparticles have slightly induced apoptosis/necrosis in HeLa cells. Nevertheless, both apoptosis and necrosis of HeLa cells can be simultaneously induced by the FA/CDs/MSN-NH_2@GEM nanoparticles with FA conjugation at the concentration used. Therefore, HeLa cells have taken up the FA/CDs/MSN-NH_2@GEM nanoparticles via FRs-mediated endocytosis and more apoptosis is induced by these nanoparticles compared with CDs/MSN-NH_2@GEM.

Cellular uptake using fluorescent microscopy

Fluorescence microscopy was used to carry out the qualitative analysis of the cellular uptake of FA/CDs/MSN-NH_2@ GEM and CDs/MSN-NH_2@ GEM by the FRs overexpressing HeLa cells via the intrinsic fluorescence characteristics of CDs. HeLa cells were treated with FA/CDs/MSN-NH_2@ GEM and CDs/MSN-NH_2@ GEM (20 µg mL^{-1}) for 3 h at 37 °C. Figure 9 displays the relative cellular uptake of FA/CDs/MSN-NH_2@ GEM and CDs/MSN-NH_2@ GEM with respect to the fluorescence intensity shown by the cells. As observed in the figure, the cellular uptake of GEM-loaded FA/CDs/MSN-NH_2 (B) is higher compared with GEM-loaded CDs/MSN-NH_2 (A) in the HeLa cells. According to the cellular imaging results, the outstanding uptake of FA/CDs/MSN-NH_2@ GEM by HeLa cell line results from FR-mediated endocytosis.

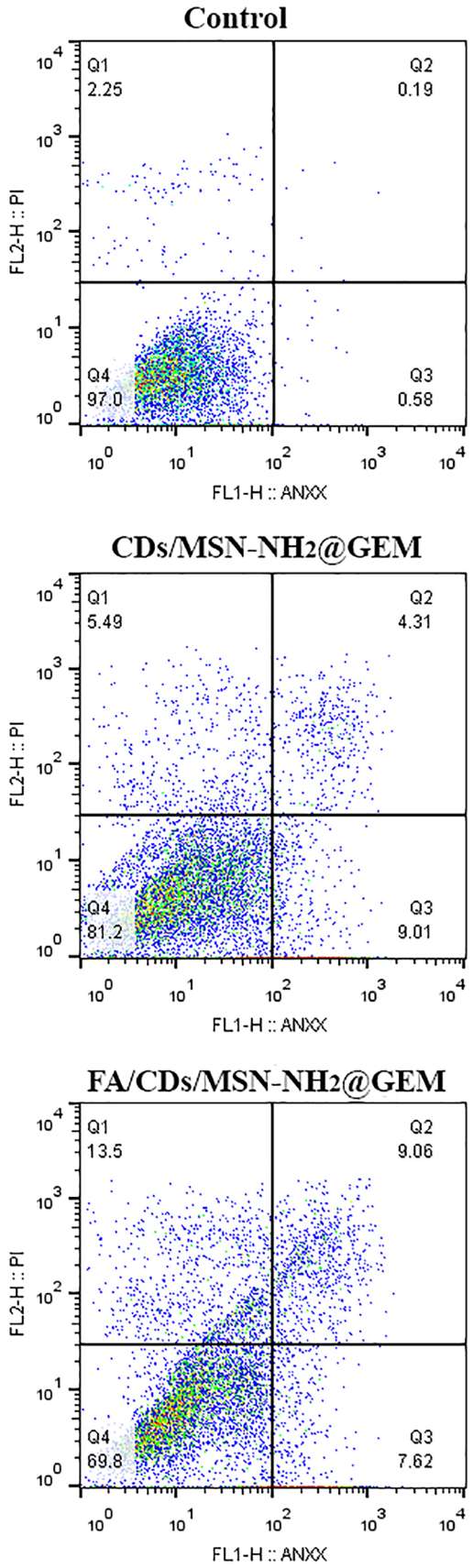

Fig. 8 Flow cytometry dot plot of **A** Control, **B** CDs/MSN-NH_2@GEM, and **C** FA/CDs/MSN-NH_2@GEM in HeLa cells

Molecular docking studies

A computational approach increasingly used in the investigation of the behavior of a drug within the appropriate target binding mode(s) of a protein is molecular docking. In addition, molecular docking studies are significant, cheap, and facile tools usually applied in drug discovery and structural molecular biology [54, 55]. Considering the importance of the interaction between any biomolecule and a drug, molecular docking studies were used to explore the interactions of the GEM with dCK and the results are displayed in Fig. 10. As illustrated in the 2D schematic interaction model, as shown in Fig. 10B, there are seven hydrogen bonds between the N1 atom of GEM and Gln 97 with 3.10 Å length, the N3 atom of GEM and Asp133 with 2.93 Å length, the O2 atom of GEM and Arg 192 with 3.27 Å length, the O2 atom of GEM and Arg 194 with 3.12 Å length, the O3 atom of GEM and Arg 194 with 2.93 Å length, the O3 atom of GEM and the Glu 197 with 3.11 Å length, also between the F1 atom of GEM and Tyr 86 with 3.07 Å length. There are four hydrophobic contact points between the GEM atoms and the amino acids of dCK, viz. (i) between C1 and C2 with Phe 134, (ii) between C2 with Phe 96, (iii) between C6 with Leu 82, and (iv) between C9 with Ile 30. These results are in the agreement with statement of Sabini and et al. [56]. Moreover, the binding free energy for the GEM with dCK was found to be − 8.2 kcal mol^{-1}.

Conclusion

In this work, an intelligent FA-targeted nanosystem with imaging capability has been developed by coating carbon dots with amine mesoporous silica. Afterward, FA has been grafted on the drug-loaded CDs/MSN-NH_2 surface. Amine-functionalized silica has been used to entrap GEM within the silica pores. Hydroxyl and carboxylic-functionalized CDs may electrostatically interact with MSN-NH_2 surfaces, thus allowing the controlled release of GEM from the pores since CDs act as gatekeepers and contrast agents. Folate-decorated nanoparticles were then formed by the secure attachment of FA as a targeting ligand to CDs/MSN-NH_2@GEM based on the interaction between FA and the folate receptors. FA/CDs/MSN-NH_2 showed some specific features such as sustained fluorescence, good monodispersity, uniform particle size and high encapsulating efficiency. pH dependence and stable drug release profiles, which can increment the therapeutic anticancer efficacy of the drug and decrease the injury to normal cells or tissues due to the acidic tumor microenvironment, were

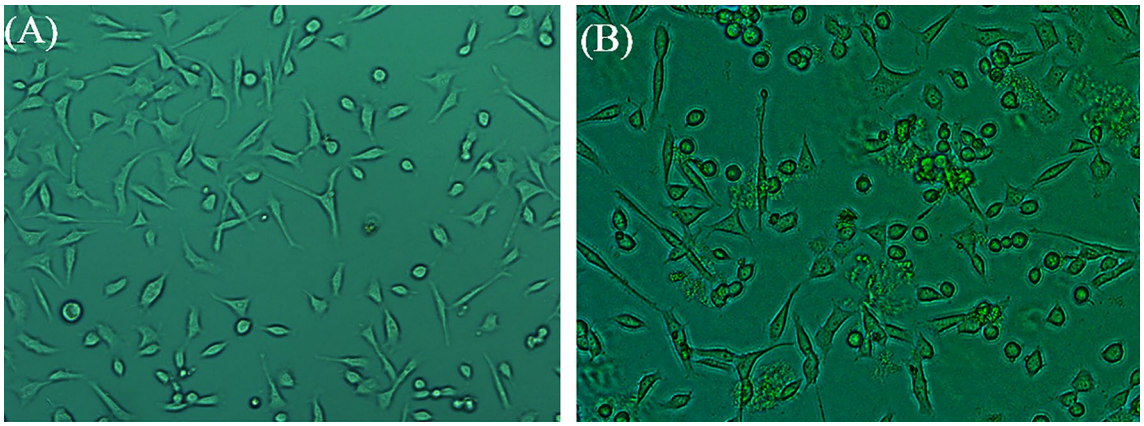

Fig. 9 Fluorescence microscopy images showing the uptake of **A** CDs/MSN-NH_2@GEM, and **B** FA/CDs/MSN-NH_2@GEM in HeLa cells

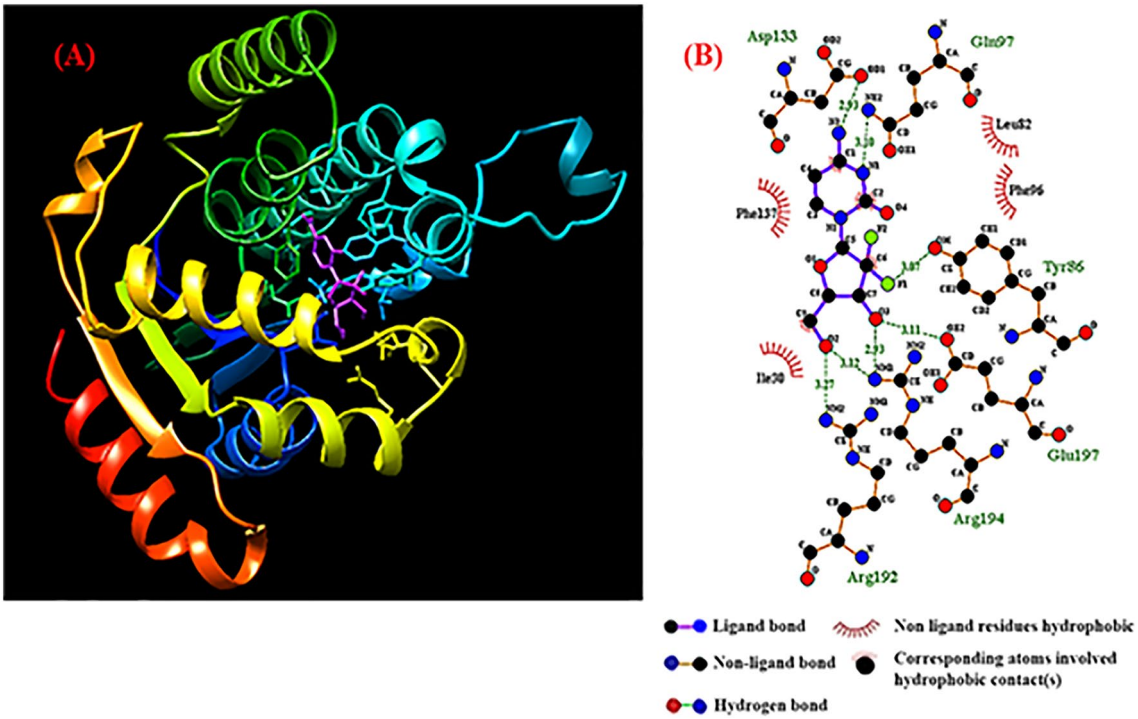

Fig. 10 **A** The molecular docking of the GEM with dCK by UCSF chimera, **B** two-dimensional interactions made using LIGPLOT+

shown by the in vitro drug release experiments. Higher cellular uptake and internalization of targeted formulation (FA/CDs/MSN-NH_2@GEM) compared with non-targeted formulation (CDs/MSN-NH_2@GEM) were shown in HeLa cells, based on the results of in vitro MTT, cell imaging, and flow cytometry experiments. The findings of this study suggest the potential application of the formulations developed with imaging ability as potent theranostic agents for diagnosis and treatment. Finally, molecular docking was applied to uncover the interactions of GEM with the dCK.

Supplementary Information The online version contains supplementary material available at https://doi.org/10.1007/s13738-023-02831-9.

Acknowledgements The authors wish to thank Iran National Science Foundation for the financial support of this work under Grant No. 97011300.

Author contributions All the authors participated in the development of the step-by-step characterization approach described, contributed to the scientific discussion, contributed to the writing of the article, and approved the manuscript.

Declarations

Conflict of interest The authors declare that the research was conducted in the absence of any commercial or financial relationships that could be construed as a potential conflict of interest.

References

1. S. Jaracz, J. Chen, L.V. Kuznetsova, I. Ojima, Bioorg. Med. Chem. **13**, 5043 (2005)
2. L. Zhou, Z. Chen, K. Dong, M. Yin, J. Ren, X. Qu, Biomaterials **35**, 8694 (2014)
3. R. Koyama, Y. Kano, K. Kikushima, A. Mizutani, Y. Soeda, K. Miura, T. Hirano, T. Nishio, W. Hakamata, Bioorg. Med. Chem. **28**, 115492 (2020)
4. E. Bagheri, L. Ansari, K. Abnous, S.M. Taghdisi, F. Charbgoo, M. Ramezani, M. Alibolandi, J. Control. Release **277**, 57 (2018)
5. T. Ahmadzada, G. Reid, D.R. McKenzie, Biophys. Rev. **10**, 69 (2018)
6. R. Chakravarty, S. Goel, H. Hong, F. Chen, H.F. Valdovinos, R. Hernandez, T.E. Barnhart, W. Cai, Nanomedicine **10**, 1233 (2015)
7. K. Zhang, C. Ding, X. Liu, J. Gao, D. Wu, Y. Qin, Y. Kong, Ceram. Int. **45**, 22603 (2019)
8. Y. He, L. Shao, Y. Hu, F. Zhao, S. Tan, D. He, A. Pan, Ceram. Int. **47**, 4572 (2021)
9. M. Babaei, K. Abnous, S.M. Taghdisi, S. Amel Farzad, M.T. Peivandi, M. Ramezani, M. Alibolandi, Nanomedicine **12**, 1261 (2017)
10. Y.-L. Sun, Y.-W. Yang, J. Control. Release **1**, e89 (2013)
11. J. Li, X. Qu, G.F. Payne, C. Zhang, Y. Zhang, J. Li, J. Ren, H. Hong, C. Liu, Adv. Funct. Mater. **25**, 1404 (2015)
12. N.Ž Knežević, B.G. Trewyn, V.S.Y. Lin, Chem. A Eur. J. **17**, 3338 (2011)
13. X. Wan, D. Wang, S. Liu, Langmuir **26**, 15574 (2010)
14. I.-C. Lin, M. Liang, T.-Y. Liu, Z. Jia, M.J. Monteiro, I. Toth, Bioorg. Med. Chem. **20**, 6862 (2012)
15. Y. He, Z. Su, L. Xue, H. Xu, C. Zhang, J. Control. Release 229 (2016) 80.
16. M. Akbarzadeh, M. Babaei, K. Abnous, S.M. Taghdisi, M.T. Peivandi, M. Ramezani, M. Alibolandi, Int. J. Pharm. **570**, 118645 (2019)
17. M. Nejabat, M. Mohammadi, K. Abnous, S.M. Taghdisi, M. Ramezani, M. Alibolandi, Carbohydr. Polym. **197**, 157 (2018)
18. H. Safardoust-Hojaghan, M. Salavati-Niasari, O. Amiri, S. Rashki, M. Ashrafi, Ceram. Int. **47**, 5187 (2021)
19. W. Li, Q. Liu, P. Zhang, L. Liu, Acta Biomater. **40**, 254 (2016)
20. C. Wang, K. Yang, X. Wei, S. Ding, F. Tian, F. Li, Ceram. Int. **44**, 22481 (2018)
21. M.P. Shirani, B. Rezaei, A.A. Ensafi, Spectrochim. Acta Part A Mol. Biomol. Spectrosc. **210**, 36 (2019)
22. Q. Duan, Y. Ma, M. Che, B. Zhang, Y. Zhang, Y. Li, W. Zhang, S. Sang, J. Drug Deliv. Sci. Technol. **49**, 527 (2019)
23. A. Hasanzadeh, M.A.M. Jahromi, A. Abdoli, H. Mohammad-Beigi, Y. Fatahi, H. Nourizadeh, H. Zare, J. Kiani, F. Radmanesh, N. Rabiee, J. Drug Deliv. Sci. Technol. **61**, 102118 (2021)
24. Q. Liu, L. Zhou, R. Lu, C. Yang, S. Wang, L. Hai, Y. Wu, Bioorg. Med. Chem. **29**, 115852 (2021)
25. L. Cerchia, Multidisciplinary Digital Publishing Institute (2018)
26. A.T. Bayraç, O.E. Akça, F.İ Eyidoğan, H.A. Öktem, J. Biosci. **43**, 97 (2018)
27. A. Yamaguchi, Y. Anami, S.Y. Ha, T.J. Roeder, W. Xiong, J. Lee, N.T. Ueno, N. Zhang, Z. An, K. Tsuchikama, Bioorg. Med. Chem. **32**, 116013 (2021)
28. V. Calzada, M. Moreno, J. Newton, J. González, M. Fernández, J.P. Gambini, M. Ibarra, A. Chabalgoity, S. Deutscher, T. Quinn, Bioorg. Med. Chem. **25**, 1163 (2017)
29. A.A. Begum, P.M. Moyle, I. Toth, Bioorg. Med. Chem. **24**, 5834 (2016)
30. S. Karamipour, M. Sadjadi, N. Farhadyar, Spectrochim. Acta Part A Mol. Biomol. Spectrosc. **148**, 146 (2015)
31. M.P. Shirani, B. Rezaei, T. Khayamian, M. Dinari, F.H. Shamili, M. Ramezani, M. Alibolandi, Mater. Sci. Eng. C **92**, 892 (2018)
32. S.-Y. Chen, P.-F. Chou, W.-K. Chan, H.-M. Lin, Ceram. Int. **43**, 2239 (2017)
33. J.-H. Lim, Y.-G. Na, H.-K. Lee, S.-J. Kim, H.-J. Lee, K.-H. Bang, M. Wang, Y.-C. Pyo, H.-W. Huh, C.-W. Cho, J. Pharm. Investig. **49**, 271 (2019)
34. X. Wang, F. Chen, S. Gou, Bioorg. Med. Chem. **29**, 115858 (2021)
35. L. de Sousa Cavalcante, G. Monteiro, Eur. J. Pharmacol. **741**, 8 (2014)
36. J. Baraniak, A. Pietkiewicz, R. Kaczmarek, E. Radzikowska, K. Kulik, K. Krolewska, M. Cieslak, A. Krakowiak, B. Nawrot, Bioorg. Med. Chem. **22**, 2133 (2014)
37. D. Dutta, L.K. Nath, P. Chakraborty, D. Dutta, J. Drug Deliv. Sci. Technol. **60**, 101981 (2020)
38. L. Martín-Banderas, E. Sáez-Fernández, M.Á. Holgado, M.M. Durán-Lobato, J.C. Prados, C. Melguizo, J.L. Arias, Int. J. Pharm. **443**, 103 (2013)
39. J.L. Arias, L.H. Reddy, P. Couvreur, Langmuir **24**, 7512 (2008)
40. X. He, Y. Zhao, D. He, K. Wang, F. Xu, J. Tang, Langmuir **28**, 12909 (2012)
41. M. Alibolandi, K. Abnous, F. Sadeghi, H. Hosseinkhani, M. Ramezani, F. Hadizadeh, Int. J. Pharm. **500**, 162 (2016)
42. O. Trott, A.J. Olson, J. Comput. Chem. **31**, 455 (2010)
43. G.M. Morris, D.S. Goodsell, R.S. Halliday, R. Huey, W.E. Hart, R.K. Belew, A.J. Olson, J. Comput. Chem. **19**, 1639 (1998)
44. R. A. Laskowski, M. B. Swindells, in *LigPlot+: Multiple Ligand–Protein Interaction Diagrams for Drug Discovery [Abstract] [Google Scholar]* (ACS Publications, 2011)
45. E.F. Pettersen, T.D. Goddard, C.C. Huang, G.S. Couch, D.M. Greenblatt, E.C. Meng, T.E. Ferrin, J. Comput. Chem. **25**, 1605 (2004)
46. N. Kazemifard, A.A. Ensafi, B. Rezaei, Food Chem. **310**, 125812 (2020)
47. M. Zahiri, M. Babaei, K. Abnous, S.M. Taghdisi, M. Ramezani, M. Alibolandi, J. Cell. Physiol. **235**, 1036 (2020)
48. A. Malfanti, I. Miletto, E. Bottinelli, D. Zonari, G. Blandino, G. Berlier, S. Arpicco, Molecules **21**, 522 (2016)
49. S.-M. Hsiao, B.-Y. Peng, Y.S. Tseng, H.-T. Liu, C.-H. Chen, H.-M. Lin, Microporous Mesoporous Mater. **250**, 210 (2017)
50. Z. Zhang, J. Jia, Y. Lai, Y. Ma, J. Weng, L. Sun, Bioorg. Med. Chem. **18**, 5528 (2010)
51. R. Lüpertz, W. Wätjen, R. Kahl, Y. Chovolou, Toxicology **271**, 115 (2010)
52. J.M. Kluza, P. Marchetti, M.-A. Gallego, S. Lancel, C. Fournier, A. Loyens, J.-C. Beauvillain, C. Bailly, Oncogene **23**, 7018 (2004)
53. S. Parveen, S.K. Sahoo, Cancer Nanotechnol. **1**, 47 (2010)
54. F. López-Vallejo, T. Caulfield, K. Martínez-Mayorga, M.A. Giulianotti, A. Nefzi, R.A. Houghten, J.L. Medina-Franco, Comb. Chem. High Throughput Screen. **14**, 475 (2011)
55. X. Meng, H. Zhang, M. Mezei, M. Cui, Curr. Computer-aided Drug Des. **7**(2), 146 (2011)
56. E. Sabini, S. Ort, C. Monnerjahn, M. Konrad, A. Lavie, Nat. Struct. Mol. Biol. **10**, 513 (2003)